LAWRENCE
LIVERMORE
NATIONAL
LABORATORY

UCRL-JRNL-214641

Imaging of Tissue Micro-Structures using a Multi-Modal Microscope Design

S. G. Demos, C. A. Lieber, B. Lin, R. Ramsamooj

August 17, 2005

Journal of Selected Topics in Quantum Electronics

Imaging of Tissue Micro-Structures using a Multi-Modal Microscope Design

Stavros G. Demos[a], Chad A. Lieber[b], Bevin Lin[b], Rajendra Ramsamooj[c]

[a] *Lawrence Livermore National Laboratory, 7000 East Avenue, Livermore, CA 94551*

[b] *UC Davis-Center for Biophotonics Science and Technology, 4800 2nd Avenue, Sacramento, CA 95817*

[c] *UC Davis Medical Center, Surgical and Transplant Pathology, 4400 V Street, Sacramento, CA 95817*

Abstract:

We investigate a microscope design that offers high signal sensitivity and hyperspectral imaging capabilities and allows for implementation of various optical imaging approaches while its operational complexity is minimized. This system utilizes long working distance microscope objectives that enable for off-axis illumination of the tissue thereby allowing for excitation at any optical wavelength and nearly eliminating spectral noise from the optical elements. Preliminary studies using human and animal tissues demonstrate the feasibility of this approach for real-time imaging of intact tissue microstructures using autofluorescence and light scattering imaging methods.

Introduction

The diagnostic gold-standard of histological evaluation of living tissues typically entails fixation, sectioning, and staining to obtain thin samples which exhibit high contrast under the microscope. While this process has led to a much deeper understanding of cellular structure, tissue sectioning is time consuming, requires removal of tissue from the patient, and has inherent sampling error. However, the most important limitation is the delay, due to processing, in providing the surgeon with clinically relevant information at the time of surgery. While frozen section analysis is an accepted practice, this technique can be used only for readily identifiable lesions. Thus, there is clearly a need to develop new methods to complement existing modalities by providing the surgeon real time information that could be used intraoperatively to identify suspect lesions.

In recent years, technological developments in laser and detection instrumentation have facilitated the exploration of optical spectroscopic techniques for the detection and monitoring of disease at the tissue level. A number of spectroscopic approaches utilizing tissue autofluorescence and/or light scattering have led the way in the development of photonic methods for in-vivo characterization of tissue structures [1-6]. Although these techniques have been explored extensively at the macroscopic level for more than a decade, their recent adaptation to the microscopic level has demonstrated their capability to image tissue micro-structures directly correlated to the histopathology of the tissue. Using confocal microscopy, tissue imaging at the microscopic level has been demonstrated using autofluorescence and light scattering [7-11]. The use of confocal microscopy in combination with fluorescence probes has enabled quantitative

measurements of dynamic events in living cells and tissues. The incorporation of time gated imaging has also presented very promising results toward the development of instrumentation that can provide histopathologic information in real time [12]. With further development, optical coherence tomography [14] and optical projection tomography [15] may be able to provide multi-spectral imaging of tissue and cell microstructures in vivo.

The development of ultrafast lasers stimulated the utilization of nonlinear interactions of ultrashort pulses with cell components. Second harmonic generation imaging arises only by molecules which are noncentrosymmetric, and hence contrast is a function of the molecular structure of the specimen and its orientation with respect to the laser beam [15]. Two-photon laser scanning microscopy offers higher resolution than confocal microscopy using infrared pulses for excitation [16]. Coherent anti-Stokes Raman scattering microscopy offers the possibility for imaging by targeting specific molecular species [17].

Although these nonlinear imaging techniques offer unique diagnostic capabilities, their implementation in a clinical environment requires the accommodation of complex instrumentation and specialized technical expertise. On the other hand, confocal microscopy is less complex but the light collection efficiency is only a small fraction of that of conventional fluorescence microscopy [18,19]. In addition, the focused beam used in confocal microscopy leads to even less efficient autofluorescence signal collection due to photo-bleaching of native tissue fluorophores and sets a limitation on the excitation energy permissible thus increasing the necessary integration times. Furthermore, it is very difficult to incorporate hyperspectral imaging techniques in a

confocal microscope without major compromises in the instrument's size and cost. Although these issues may be easily resolvable for some applications, the in-vivo application of these advanced microscopies in a clinical setting may be proven challenging.

One may then consider the possibility of developing a microscope system that takes advantage of the benefits of multi-dimensional spectroscopic imaging at the micro scale but does not incorporate the complexity of nonlinear microscopy or the signal loss of confocal microscopy. This concept has been the motivation for this work. More specifically, we have developed a conventional microscope design that incorporates hyperspectral imaging techniques and a plurality of imaging methods while offering high spatial resolution and optimized signal sensitivity for fast image acquisition. Additionally, by using off-axis illumination, spectral noise from the system's optical elements was reduced or eliminated, thereby increasing signal-to-noise and spectral purity. Using this system, we have carried out a number of experiments to demonstrate high-resolution imaging of microstructures in tissues using linear spectral imaging methods. The microscope system described in this work is intended to be a prototype platform, such that various imaging modalities can be quickly compared for their ability to provide contrast and image tissue microstructures. Those modalities most relevant for the particular tissue system can then be incorporated into a portable (endoscopic, fiber-optic, etc.) system for clinical use.

2. Experimental methods

Figure 1 shows a schematic diagram of the microscopic imaging system consisting of a portable unit and an external optical parametric oscillator (OPO) tunable laser. The imaging system located in the portable unit is equipped with long working distance microscope objectives followed by a zoom lens which is used to relay the image into a back-illuminated, liquid nitrogen cooled CCD detector. A filter assembly is located in front of the CCD in order to position the desirable optical filters for the selection of the spectral window used in each imaging experiment. In addition, a polarizer can also be inserted for polarization sensitive experiments. The large numerical apertures of the microscope objectives offer high light collection efficiency. This microscope design has been used previously in a different imaging arrangement to study fluorescing defects located in the bulk of optical materials [20]. The optimal spatial resolution is 1-μm using a X20 or higher magnification microscope objective.

The portable unit also contains a set of low-power CW lasers consisted of a Helium-Cadmium laser (325-nm), a Helium-Neon laser (632.8-nm) and four compact diode-pumped solid state lasers operating at 266-nm, 355-nm, 408-nm and 532-nm. The laser beams are delivered to the sample using optical fibers and appropriate optics to enlarge their diameter so that the imaged area is exposed to the nearly uniform light intensity of the center portion of each beam. The illumination light used in the light scattering experiments is delivered to the sample using a fiber bundle coupled to a white light source. The external (to the portable unit) laser source is an OPO pumped by an Nd:YAG laser operating at 355-nm and equipped with a second harmonic generation

crystal. This system is tunable from 250 to 340-nm and 410 to 1000-nm and is used in this work as the excitation source in autofluorescence experiments.

Autofluorescence images of fresh human tissue specimens obtained following surgical treatment as well as animal tissues were acquired using various excitation wavelengths and emission spectral bands. Kidney is a tissue system that has a well-defined structure in the microscopic level where cells on the order of 10-μm in diameter are forming tubules with diameters of 50 to 80-μm. For this reason, we used kidney tissue in this work as the primary model to demonstrate with our system spectroscopic imaging at the microscopic level.

3. Experimental results

Figure 2a shows the autofluorescence image of a cross section of a human kidney specimen using the X10 objective with 260-nm excitation and 400-1000-nm (using a long pass filter) collection. The specimen is 4-mm thick and was obtained fresh from surgery without additional sample preparation. The normal tubules are visible even to the untrained eye in the center of this image. Due to the limited depth of focus of the objective and the uneven surface of the sample, some of the features in this image are slightly out of focus. The inset in Figure 2a illustrates the histological structure of the tubules of the kidney from the image of an H&E stained section. Each tubule is composed of a single layer of cells. The nuclei of the cells appear as darker features in the H&E stained section.

The features on the left side of the autofluorescence image shown in Figure 2a are cross sections of tubules cut by a surgical knife. Figure 2b shows a close up image

of these tubules near the location indicated by the arrow. This image shows with high resolution the sectioned tubules while the thickness of the tubules is about 10-μm, equivalent to a single cell layer. The average pixel intensity of the digitized image of the ≈ 10 μm thick body of the tubule is 40-60% higher than the intensity in the middle of the tubule, providing contrast to visualize the tubular parenchyma microstructures. A careful examination of the cross section of the tubules reveals the presence of darker features that have the size and relative distance of the nuclei seen in the H&E stain. These darker features are also visible in the autofluorescence image of the intact tubules (shown by an arrow in Figure 2a) under 260-nm excitation as demonstrated in Figure 2c. This higher resolution image of a single tubule clearly shows the darker features located 10 to 15-μm from each other. These features exhibit average intensities approximately 20% lower than the surrounding area of the tubule's surface and are presumed to be the nuclei of the tubular cells.

The autofluorescence image under 260-nm excitation arises predominantly from tryptophan emission. An image of the tubules from the same specimen under 330-nm excitation is shown in Figure 3. The origin of the emission under this excitation is expected to be NADH [21]. Figure 3 demonstrates that the tubules are clearly visible under 330-nm excitation but the appearance of the tubules in this image is different compared to that under 260-nm excitation. More specifically, the darker features under 260-nm excitation (which were assumed to be the cells' nuclei) are not visible under 330-nm excitation. Instead, the emission intensity within the tubules is uneven and features that exhibit higher intensity having diameter on the order of a few microns are visible. We also recorded images using excitation wavelengths from 250-nm to 340-nm.

In general, images under 250-nm to 280-nm excitation appear to be similar to those shown in Figure 2. Images obtained under 300-nm to 340-nm excitation were similar to that shown in Figure 3. Similar experiments were performed using two more human kidneys, kidneys obtained from experimental rats, as well as bovine and porcine kidneys obtained from the market. All results were qualitatively the same as those discussed above.

We have recently discussed elsewhere that NIR auto-fluorescence under long-wavelength excitation (green or red) offers contrast between normal and cancer tissue components depending on the type of tissue or organ [22]. In the case of kidney cancer, the tumor appears as a darker feature compared to normal tissue. We investigated this imaging approach, which has been explored only in the macroscopic field, using the high resolution imaging instrumentation discussed in this work. Figure 4a shows the auto-fluorescence image of human kidney using a 670-nm long pass filter and 532-nm excitation. The specimen is 5-mm thick and was obtained fresh from surgery. The exposure time was 1 second under 7-mW laser illumination. The tubules are clearly visible again but the origin of the autofluorescence is not clear. The bright features that contribute to the visualization of the tubules have intensities 20-50% higher than the rest of the image. It was not possible from pathology to identify the nature of these features. Figure 4b shows the NIR auto-fluorescence image of human kidney in an area where tumor (papillary renal cell carcinoma) interfaces with the normal tissue. Figure 4c shows a contrast enhanced H&E stained section of the same region, in which the tumor is on the upper side, the lower side is normal kidney parenchyma, and in the middle is normal tissue compressed by the expanding tumor. In the

autofluorescence image shown in Figure 4b, the tumor appears as a darker feature while the tubules are brighter. A higher magnification image (110 X 140 μm) of a section from the tumor is shown in Figure 4e. This image shows that the tumor has irregular texture with no organization. For comparison, an image (190 X 220 μm) from normal kidney is shown in Figure 4d. The average intensity of the normal tissue in this image is ≈18% higher than that of the tumor tissue. The compression of the tubules by the tumor at the interface is also clearly visible in the auto-fluorescence image shown in Figure 4b and appears as an area of enhanced emission having about twice the intensity of the tumor area due to the compaction of the tissue and the tubules that are collapsing and respective enhancement of concentration of fluorophores.

Figure 5 shows the autofluorescence image of a 650 X 500 μm section from the inner surface of porcine small intestine. The excitation wavelength was 280-nm and the image was recorded using the X20 microscope objective. The epithelial cells are visible in this image as round features with diameter of about 10-μm. Best contrast using autofluorescence imaging of small intestine cells was achieved using 280-nm excitation but the cells were also visible under all UV excitations as well as the compact 408-nm laser. We have performed similar experiments in other tissues and organs such as liver, pancreas, colon and breast. In all cases we can see features that can be directly related to the microstructure of the tissue.

Attempts to utilize light scattering techniques to visualize the microstructures shown in Figure 2 through 5 were unsuccessful. The corresponding light scattering images of these Figures contained no recognizable features, just a white background. We found, however, that some relatively large structures (such as fat cells) can be

imaged using light scattering. As an example, we show in Figure 6 light scattering microscopic images from a 850 X 1000 μm section of a human breast specimen at the intersection between normal adipose (lower left) and tumor tissue (infiltrating ductal carcinoma). This specimen was obtained fresh following lumpectomy.

Figure 6a shows the unpolarized light scattering image of this specimen using white light illumination and a 450±20-nm narrow band filter in front of the CCD camera. The exposure time was 0.2 seconds. As can be seen in the Figure, the tissue components are distinctly different, permitting detection of the tumor edge (margin) with high spatial resolution. The average image intensity of the normal tissue is ≈0.36 to that of the cancer tissue. Figure 6b shows an image of the same site under same conditions but using an 800±40-nm filter for image formation. This image provides a lower contrast between normal adipose and cancer tissue. The average intensity in the image of the adipose tissue was measured to be ≈0.88 to that of the cancer tissue. Figure 6c was obtained by dividing, pixel by pixel, the light scattering image obtained under white light using a narrow band filter at 450±20-nm by the image obtained using an 800±40-nm filter. In this image, the contrast is further enhanced taking advantage of the spectral differences of the light scattering intensity from these tissue components.

The high spatial resolution in delineating the tumor's margins is best depicted in Figure 6d where a 360 X 300 μm section is shown at the intersection of the tumor with the normal tissue The outline of individual adipocytes is easily appreciated. Additionally, the first row of normal adipose cells that are in contact with the tumor are clearly visible. The bright features in the normal tissue are consistent with the size and location of the nuclei of the adipose cells. In these images the tumor is clearly separated from the

normal adipose tissue but the challenge would be to separate cancer form normal connective tissue. In such a case, light scattering imaging may not be sufficient and may require the utilization of autofluorescence imaging. Work to address this issue is in progress.

4. Discussion

The multimodal optical imaging experimental system described in this work has been designed with future portable application in mind. All tissue samples imaged with this system and shown in the figures were intact and unprocessed specimens simulating the conditions that would be encountered in a clinical setting. The methods found using this platform system to provide optimum contrast between pathologically relevant microstructures of a particular tissue system can be readily incorporated in endoscopic, fiber optic, or micro optic-based handheld systems for clinical use.

The main strength of this microscope design is that it can incorporate a large variety of spectral imaging techniques including the ability to use any available excitation wavelength, utilize fluorescence or light scattering spectral imaging, and incorporate polarization techniques without having to make any modifications to the instrument. This feature allows the instrument to be quickly adapted to various imaging tasks, and can easily be operated by an unskilled user.

Autofluorescence microscopy and spectral and polarization-sensitive light scattering microscopy are the main imaging methods that can be implemented with our microscope system. Autofluorescence microscopy can take advantage of the variation of tissue chromophores in the microscopic level to image subcellular components and

tissue microstructures as demonstrated in Figures 2 through 5. Light scattering techniques can take advantage of the variation of the scattering intensity of tissue microstructures as a function of the illumination wavelength, which depends on their index of refraction and size. Polarization can be used to further enhance these differences and can also be used to remove signal arising from out of focus features located below the image plane (just below the surface of the tissue) that will be depolarized or less polarized due to scattering [23]. Time gated imaging can be added to further enhance contrast between different tissue components [12].

The experimental system described in this work is composed of a portable unit and an OPO laser system. The OPO laser provides continuously variable excitation from the UV to the NIR spectral region to reveal the optimal excitation conditions for best image contrast and visualization of microstructures of interest in various tissue types. However, upon determination of the most successful approaches to image a particular tissue system, the excitation source can be replaced with a set of portable compact lasers such as those already incorporated into the portable unit. The portable unit was built so that it can be transferred to an animal facility to perform in vivo experiments in small animal models.

A microscope system suitable for in vivo application in a clinical setting should be able to provide: a) contrast between components of intact tissue to reveal histopathologic information, b) sufficiently high spatial resolution to separate structures and components of interest and, c) fast image acquisition for real time imaging of an object (tissue component or organ) that may be continuously moving due to heartbeat and blood flow. We believe that this microscope design offers the promise to fulfill all

these objectives. Our preliminary results are strongly suggestive that our experimental microscope system can provide high resolution spectroscopic images of superficial tissue microstructures that are related to the pathologic state of the tissue. Furthermore, the image acquisition time can be very fast due to optimization of the light collection efficiency. All autofluorescence images shown were captured with exposure times of 1 second under laser irradiation that did not exceed 5-mW/mm^2 in the visible and 0.5-mW/mm^2 in the ultraviolet spectrum.

The image quality of an in vivo microscope system depends not only on the designing characteristics of the optical components but also the degree to which the object being imaged can be kept immobilized with respect to the imaging system (microscope) during image acquisition. Obviously, this is a problem when imaging *in vivo*, due to intrinsic micro- and macro-movements of the vasculature, musculature, etc. An effective solution to this problem is to acquire an image much faster than the tissue can move beyond the instrument's specified spatial resolution of- and relative to the imaging system. This can be achieved using pulsed illumination, such that the image is acquired from exposure to a single pulse. In this case, the effective image acquisition time of an autofluorescence image is on the order of a few nanoseconds (determined by the longer of the emission lifetime or laser pulselength). For example, using illumination of ≈ 0.5 mJ/mm^2 in the UV obtained from a Q-switched laser, our results suggest that this photoexcitation is sufficient to acquire a high quality image of the tissue. In this case, even if we assume that the relative microscope-tissue speed of motion is an extreme value of 10 cm/sec, the relative movement during a 10 ns time interval is about 1 nanometer. Consequently, pulsed illumination shorter than about 10 μsec offers

image acquisition fast enough to eliminate any loss in spatial resolution during in vivo application.

Since the imaging elements of this design are separated from the optical elements delivering the excitation light (via off-axis illumination), excitation at multiple wavelengths is unrestricted by chromatic aberrations and the transmissive properties of optical components. This approach also eliminates any background signal (noise) arising from the optical elements, an issue most notable under UV excitation. Furthermore, off-axis illumination is capable of providing topological images of tissue, based on shadowing of the illumination light by microstructures in the tissue. This effect is maximized under UV excitation due to the smaller photon penetration depth.

A key disadvantage of the microscope design utilized in this work when compared to confocal or nonlinear microscopies is that it has no image sectioning capability. This feature is sacrificed in order to achieve optimal signal collection for fast image acquisition times and incorporation of different imaging methods that can be easily exchanged during operation. However, structured illumination can be used to add sectioning capabilities and enhance the image contrast of superficial tissue microstructures [12], but important aspects of this design (such as the system's complexity, adaptability for endoscopic designs and the speed of image acquisition) may be compromised.

Our experimental results indicate that tissue cells and microstructures can be quickly imaged microscopically using their autofluorescence under UV excitation. We have tested various tissue systems of interest such as colon, liver, pancreas, bladder, esophagus and normal tissue structures were clearly visible in all cases. A clear benefit

in using UV excitation is that the short photon penetration depth due absorption by tissue facilitates a low signal arising from the subsurface tissue layers providing for enhanced signal of the in-focus features on the surface layer of the tissue. On the other hand, imaging in the visible spectrum may offer valuable information to highlight disease specific optical signatures as shown in Figure 4. In these cases, imaging using UV excitation complemented by disease specific imaging in the visible or NIR may offer sufficient information for histopathologic evaluation and accurate delineation of tumor's margins.

The knowledge obtained from the experimental system described in this work can provide the basis for the development of a microscopic imaging instrument that can assist during surgery by providing pathologically relevant tissue information in real time. This method may be best suited as a complementary tool to a low spatial resolution optical modality that rapidly provides examination at the tissue level and may utilize native contrast mechanisms or contrast agents. In this arrangement, a high-resolution imaging instrument can assist to better delineate the tumor's margins and as a screening tool of small tumors not visible in the macroscopic field. It may also be used as a monitoring tool of tissues or organs during treatment or exposure to adverse conditions by employing an array of spectroscopic methods that can provide information at the microscopic level (e.g. change of tissue chromophore properties, location of uptake of contrast agent, cell swelling etc).

Acknowledgements

This work was performed in part at UC, Lawrence Livermore National Laboratory under the auspices of the U.S. Department of Energy under Contract W-7405-Eng-48. This research is supported by funding from the California Breast Cancer Research Program and the National Science Foundation. The Center for Biophotonics, an NSF Science and Technology Center, is managed by the University of California, Davis, under Cooperative Agreement No. PHY 0120999.

References

1. R. R. Alfano, B. Tata, J. Cordero, P. Tomashefsky, F. W. Longo. M. A. Alfano, "Laser induced fluorescence spectroscopy from native cancerous and normal tissues", IEEE J. Quantum Electron., **20**, 1507-1511 (1984)
2. C. R. Kapadia, F. W. Cutruzzola, K. M. O'Brien, M. L. Stetz, R. Enriquez, L. I. Deckelbaum, "Laser-induces fluorescence spectroscopy of human colonic mucosa detection of adenomatous transformation", Gastroenterology, **99**, 150-157 (1990)
3. R. R. Kortum, R. P. Rava, R. E. Petras, M. Fitzmaurice, M. Sivak, M. S. Feld, "Spectroscopic diagnosis of colonic dysphasia", Photochem & Photobio., **53**, 777-786, (1991)
4. C. J. Frank, D. C. Redd, T. S. Gansler, R. L. McCreery, "Characterization of human breast specimens with Near-IR Raman spectroscopy", Anal. Chem., **66**, 319-326 (1994)
5. N. Ramanujam , M.F. Mitchell, A. MahadevanJansen, S.L. Thomsen , G. Staerkel, A. Malpica, T. Wright, N. Atkinson, R. Richards-Kortum, "Cervical precancer detection using a multivariate statistical algorithm based on laser-induced fluorescence spectra at multiple excitation wavelengths", Photochemistry and Photobiology, **64**, 720-735 (1996)
6. V. Backman, M.B. Wallace, L.T. Perelman, J.T. Arendt, R. Gurjar, M.G. Muller, Q. Zhang, G. Zonios, E. Kline, T. McGillican, S. Shapshay, T. Valdez, K. Badizadegan, J.M. Crawford, M. Fitzmaurice, S. Kabani, H.S. Levin, M. Seiler,

R.R. Dasari, I. Itzkan, J. Van Dam, M.S. Feld, “Detection of preinvasive cancer cells”, Nature, **406**, 35-36 (2000)

7. W. Hsing-Wen, J. Willis, M.J.F. Canto, M.V. Jr. Sivak, J.A. Izatt, “Quantitative laser scanning confocal autofluorescence microscopy of normal, premalignant, and malignant colonic tissues”, IEEE Transactions on Biom. Engineering, **46**, 101246-52 (1999)
8. I. Pavlova, K. Sokolov, R. Drezek, A. Malpica, M. Follen, R. Richards-Kortum, Microanatomical and biochemical origins of normal and precancerous cervical autofluorescence using laser-scanning fluorescence confocal microscopy, Photochem Photobiol., **77**, 550-555 (2003)
9. Z.W. Huang, W. Zheng, S.S. Xie, R. Chen, H.S. Zeng, D.I. McLean, H. Lui, “Laser-induced autofluorescence microscopy of normal and tumor human colonic tissue”, Int. J.l Of Oncology, **24** , 59-63 (2004)
10. J. V. Jester, P. M. Andrews, W. M. Petroll, M. A. Lemp, H. D. Cavanagh, “In vivo, real-time confocal imaging”, J Electron Microsc Tech. 18, 50-60, (1991).
11. M. Rajadhyaksha, G. Menaker, T. Flotte, P. J. Dwyer, S. Gonzalez., “Confocal examination of nonmelanoma cancers in thick skin excisions to potentially guide Mohs micrographic surgery without frozen histopathology”, J. of Investigative Dermatology, **117**, 1137-1143 (2001).
12. J. Siegel, D.S. Elson, S.E.D. Webb, D. Parsons-Karavassilis, S. Leveque-Fort, M.J. Cole, M.J. Lever, P.M.W. French, M.A.A. Neil, R. Juskaitis, L.O. Sucharov, T. Wilson, “Whole-field five-dimensional fluorescence microscopy combining

lifetime and spectral resolution with optical sectioning", Opt. Lett., **26**, 1338-40 (2001)

13. N. Nishizawa, Y. Chen, P. Hsiung, E.P. Ippen, J. G. Fujimoto, "Real-time, ultrahigh-resolution, optical coherence tomography with an all-fiber, femtosecond fiber laser continuum at 1.5 micron", Opt Lett. **29**, 2846, (2004).
14. J. Sharpe, U. Ahlgren, P. Perry, B. Hill, A. Ross, J. Hecksher-Sorensen, R. Baldock, D. Davidson, "Optical Projection Tomography as a Tool for 3D Microscopy and Gene Expression Studies", Science, **296** , 541, (2002)
15. J. N. Gannaway, C. J. R. Sheppard, "Second harmonic imaging in the scanning optical microscope", Optical and Quantum Electronics, **10**, 435-439 (1978).
16. W. Denk, J. H. Strickler, W. W. Webb, "Two-photon Laser scanning fluorescence microscopy", Science, **248**, 73-76 (1990).
17. A.Zumbusch, G. R. Holtom, and X. S. Xie, "Three-dimensional vibrational imaging by coherent anti-Stokes Raman scattering", Phys. Rev. Lett., **82**, 4142-4145 (1999).
18. D. R. Sandison and W. W. Webb, "Background rejection and signal-to-noise optimization in confocal and alternative fluorescence microscopes", Appl. Opt. **33**, 603-615 (1994).
19. K. S. Wells, D. R. Sandison, J. Stricker and W. W. Webb, "Quantitative fluorescence imaging with laser scanning confocal microscopy", The Handbook of Biological Confocal Microscopy, J. B. Pawley, Eds, (IMR Press, 1989).

20. S. G. Demos, M. Staggs, M. Yan, H. B. Radousky and J. J. De Yoreo Microscopic fluorescence imaging of bulk defect clusters in KH2PO4 crystals, Opt. Lett., **24**, 268, 1999.
21. G. A Wagnieres, W. M. Star and B. C. Wilson, "In vivo fluorescence spectroscopy and imaging for oncological applications," Photochem. Photobiol., **68**, 603-632 (1998).
22. S. G. Demos, R. Gandour-Edwards, R. Ramsamooj, R. deVere White, “Near infrared autofluorescence imaging for detection of cancer”, J. Biom. Opt., **9**, 587-592 (2004)
23. S. G. Demos and R.R. Alfano, “Optical Polarization Imaging” Applied Optics, **36**, 150-155 (1997).

Figure Captions

Figure 1. Schematic layout of the key optical components of prototype hyperspectral microscope

Figure 2. a) Microscopic autofluorescence image of normal human kidney under 260-nm excitation. Inset illustrates the histologic structure of two kidney tubules from an H&E stained section. b) Image of a set of sliced tubules by the surgical knife. c) Image of an intact tubule. Dark features are believed to be the cell nuclei.

Figure 3. Microscopic autofluorescence image of a 360 X 340 μm section of normal human kidney under 330-nm excitation.

Figure 4. a) NIR autofluorescence image of a 960 X 600 μm section of normal human kidney tissue under 532-nm excitation and b) in the area of tumor interface with the normal tissue. c) Contrast enhanced H&E stains of the tumor-normal tissue interface. d) Higher magnification image of the normal kidney tissue and e) of the tumor.

Figure 5. Autofluorescence image of 650 X 500 μm section of the interior surface of porcine small intestine recorded under 280-nm excitation.

Figure 6. Light scattering microscopic images of a 1000 X 850 μm section of a human breast specimen at the intersection of normal adipose and tumor tissue using a) an 450±20-nm filter, b) an 800±40-nm filter and, c) Ratio image. d) A higher magnification ratio image of a 300 X 360 μm section.

Figure 1:

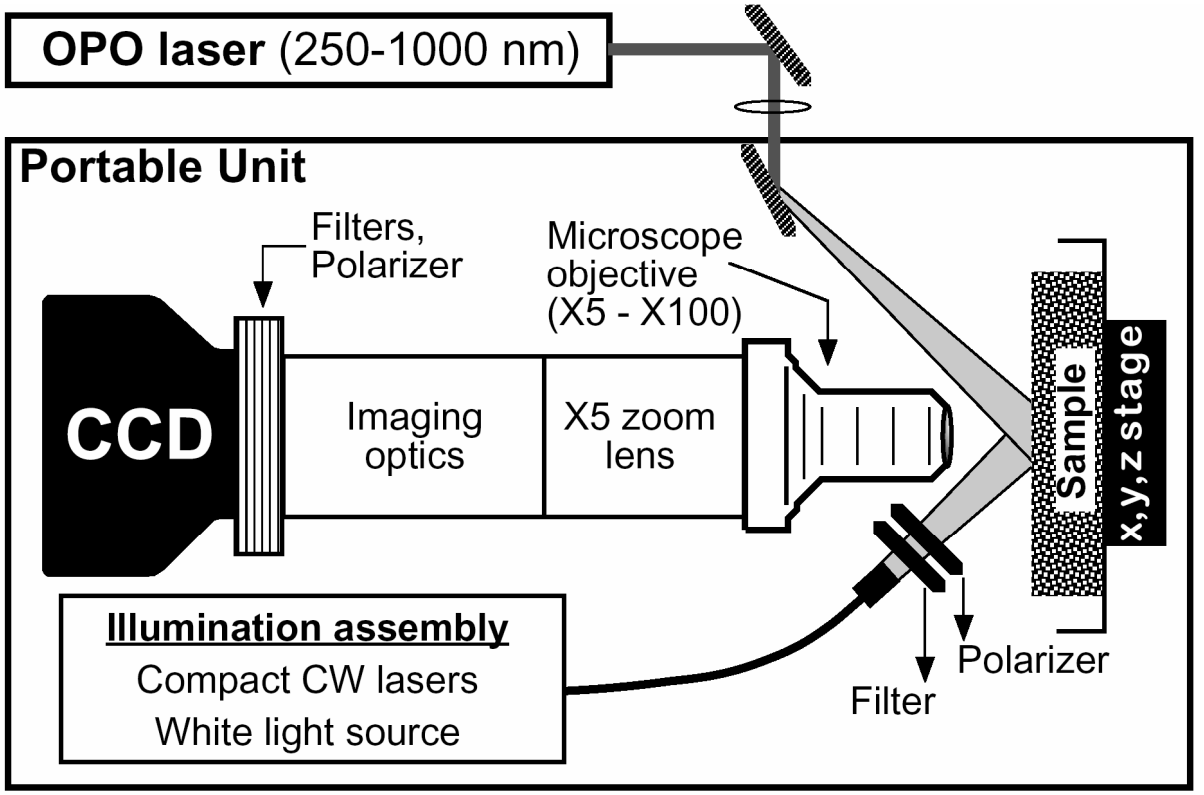
OPO laser (250-1000 nm)
Portable Unit
Filters,
Polarizer
Microscope
objective
(X5 - X100)
CCD
Imaging
optics
X5 zoom
lens
Sample
x,y,z stage
Illumination assembly
Compact CW lasers
White light source
Polarizer
Filter

Figure 2:

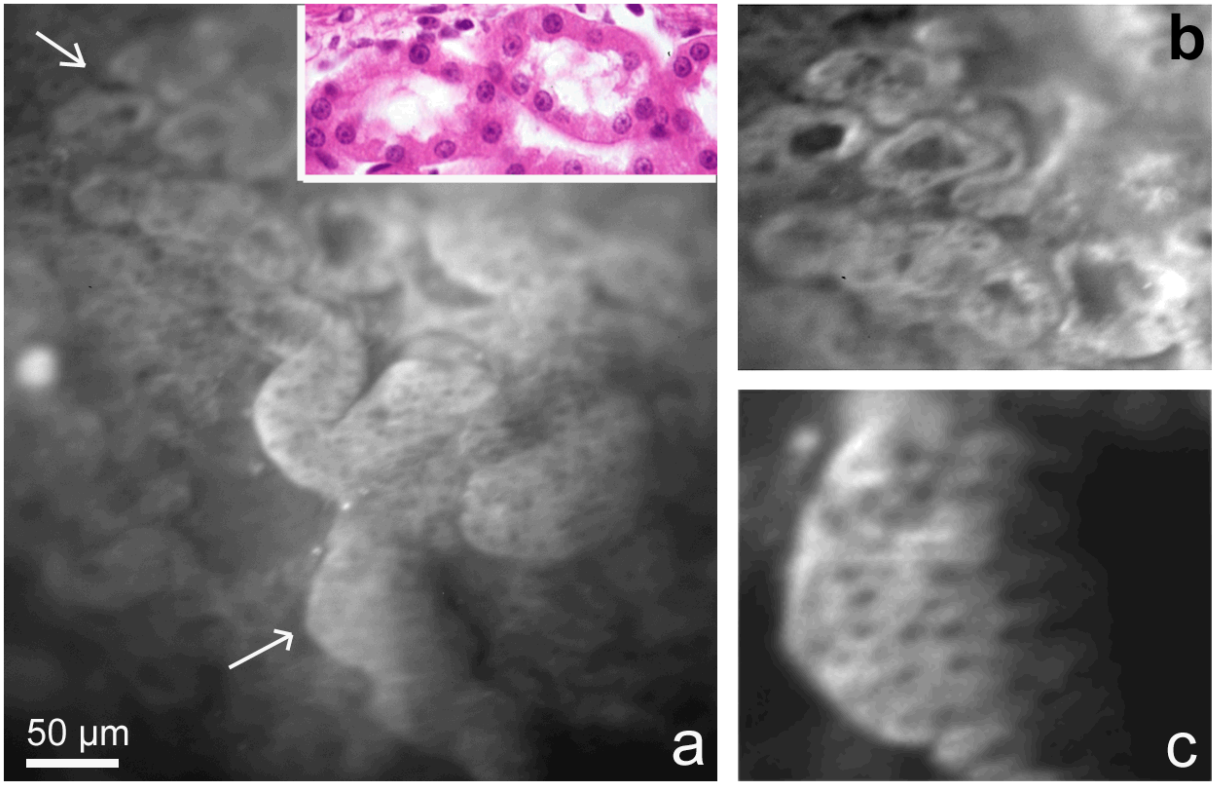

Figure 3:

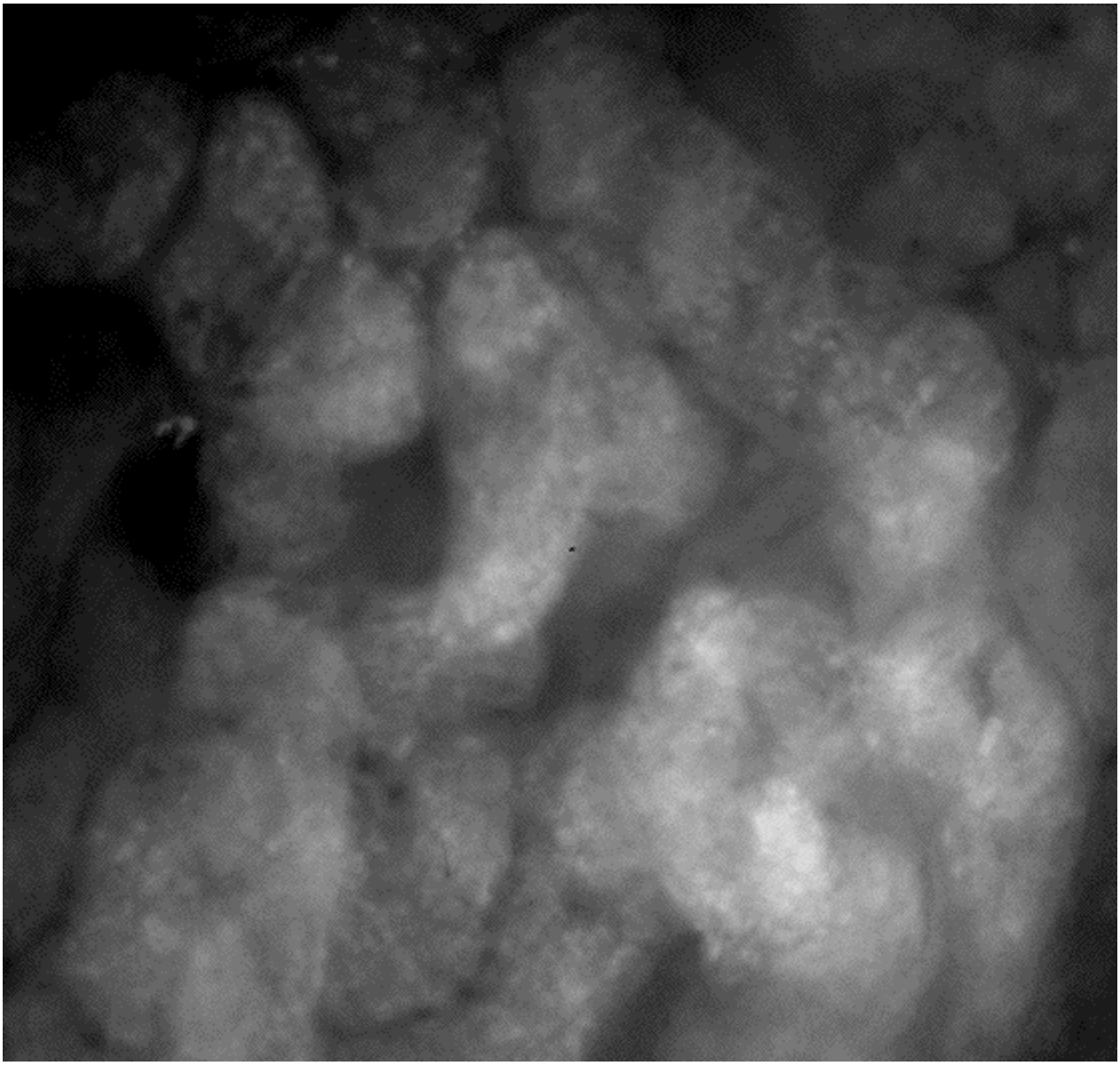

Figure 4:

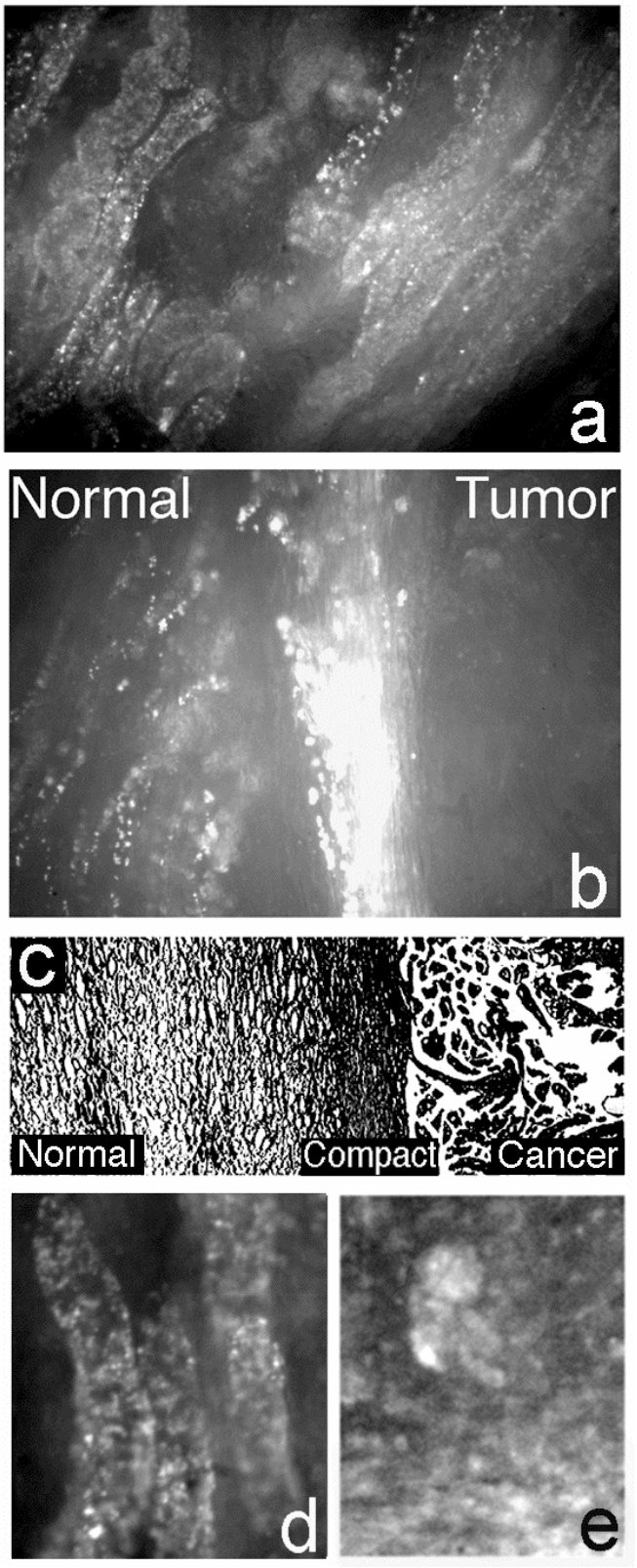

Figure 5:

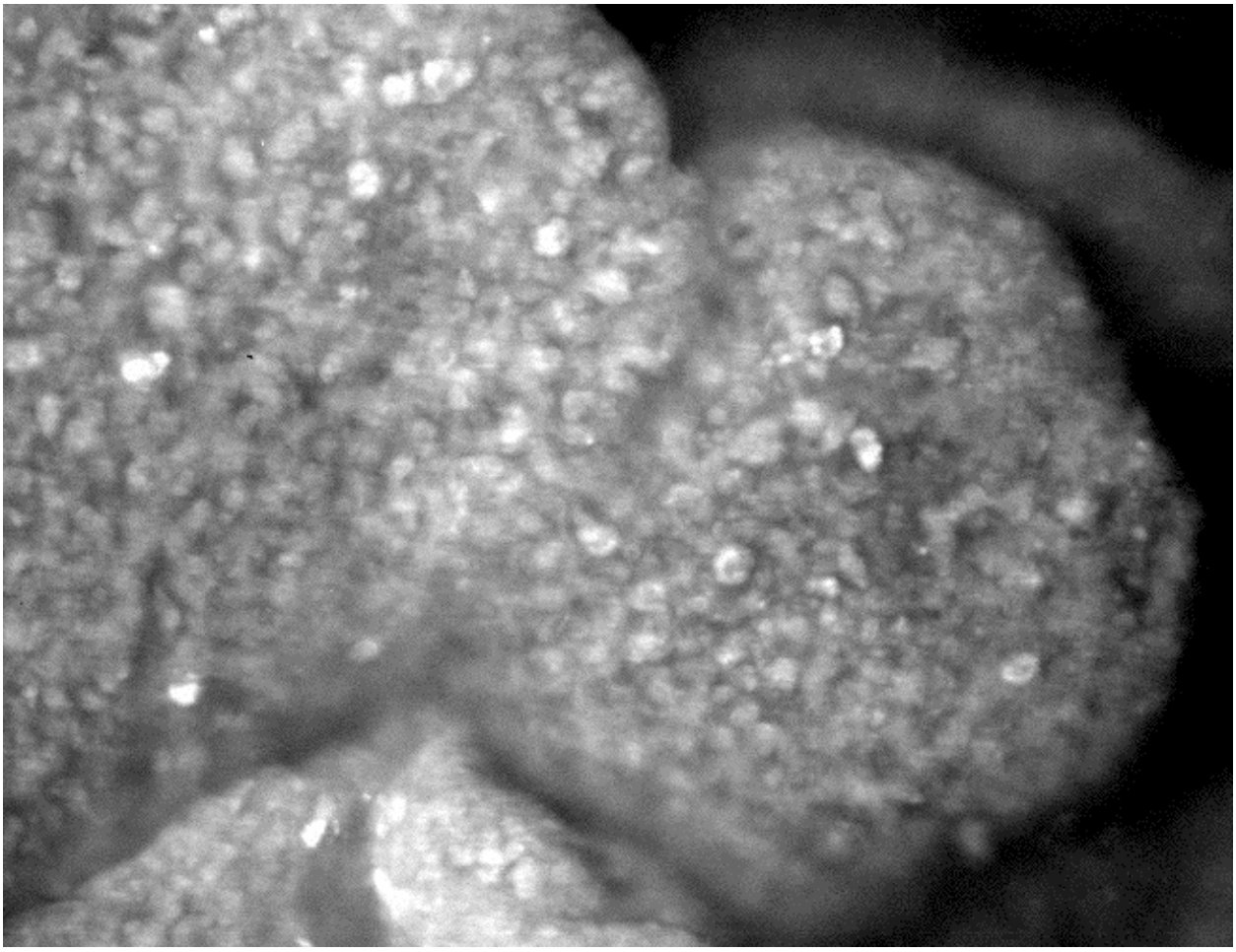

Figure 6: